Atmos. Meas. Tech., 10, 3359–3373, 2017
https://doi.org/10.5194/amt-10-3359-2017

Atmospheric Measurement Techniques
Open Access
EGU

Tropospheric ozone profiles by DIAL at Maïdo Observatory (Reunion Island): system description, instrumental performance and result comparison with ozone external data set

Valentin Duflot[1,2], Jean-Luc Baray[3], Guillaume Payen[2], Nicolas Marquestaut[2], Francoise Posny[1], Jean-Marc Metzger[2], Bavo Langerock[4], Corinne Vigouroux[4], Juliette Hadji-Lazaro[5], Thierry Portafaix[1], Martine De Mazière[4], Pierre-Francois Coheur[6], Cathy Clerbaux[5,6], and Jean-Pierre Cammas[1,2]

[1]Laboratoire de l'Atmosphère et des Cyclones (LACy), UMR8105, Saint-Denis, Réunion, France
[2]Observatoire des Sciences de l'Univers de La Réunion (OSUR), UMS3365, Saint-Denis, Réunion, France
[3]Laboratoire de Météorologie Physique (LaMP), UMR6016, Observatoire de Physique du Globe de Clermont-Ferrand, CNRS - Université Blaise Pascal, Clermont-Ferrand, France
[4]Royal Belgian Institute for Space Aeronomy (BIRA-IASB), 3, Av. Circulaire, 1180, Brussels, Belgium
[5]LATMOS/IPSL, UPMC Univ. Paris 06 Sorbonne Universités, UVSQ, CNRS, Paris, France
[6]Spectroscopie de l'Atmosphère, Service de Chimie Quantique et Photophysique, Université Libre de Bruxelles (ULB), Brussels, Belgium

Correspondence to: Valentin Duflot (valentin.duflot@univ-reunion.fr)

Received: 9 December 2016 – Discussion started: 25 January 2017
Revised: 13 July 2017 – Accepted: 24 July 2017 – Published: 15 September 2017

Abstract. In order to recognize the importance of ozone (O_3) in the troposphere and lower stratosphere in the tropics, a DIAL (differential absorption lidar) tropospheric O_3 lidar system (LIO3T$_{UR}$) was developed and installed at the Université de la Réunion campus site (close to the sea) on Reunion Island (southern tropics) in 1998. From 1998 to 2010, it acquired 427 O_3 profiles from the low to the upper troposphere and has been central to several studies. In 2012, the system was moved up to the new Maïdo Observatory facility (2160 m a.m.s.l. – metres above mean sea level) where it started operation in February 2013. The current system (LIO3T) configuration generates a 266 nm beam obtained with the fourth harmonic of a Nd:YAG laser sent into a Raman cell filled up with deuterium (using helium as buffer gas), generating the 289 and 316 nm beams to enable the use of the DIAL method for O_3 profile measurements. The optimal range for the actual system is 6–19 km a.m.s.l., depending on the instrumental and atmospheric conditions. For a 1 h integration time, vertical resolution varies from 0.7 km at 6 km a.m.s.l. to 1.3 km at 19 km a.m.s.l., and mean uncertainty within the 6–19 km range is between 6 and 13 %. Comparisons with eight electrochemical concentration cell (ECC) sondes simultaneously launched from the Maïdo Observatory show good agreement between data sets with a 6.8 % mean absolute relative difference (D) between 6 and 17 km a.m.s.l. (LIO3T lower than ECC). Comparisons with 37 ECC sondes launched from the nearby Gillot site during the daytime in a ±24 h window around lidar shooting result in a 9.4 % D between 6 and 19 km a.m.s.l. (LIO3T lower than ECC). Comparisons with 11 ground-based Network for Detection of Atmospheric Composition Change (NDACC) Fourier transform infrared (FTIR) spectrometer measurements acquired during the daytime in a ±24 h window around lidar shooting show good agreement between data sets with a D of 11.8 % for the 8.5–16 km partial column (LIO3T higher than FTIR), and comparisons with 39 simultaneous Infrared Atmospheric Sounding Interferometer (IASI) observations over Reunion Island show good agreement between data sets with a D of 11.3 % for the 6–16 km partial column (LIO3T higher than IASI). ECC, LIO3T$_{UR}$ and LIO3T O_3 monthly climatologies all exhibit the same range of values and patterns. In particular, the Southern Hemisphere biomass burning seasonal enhancement and the ozonopause altitude decrease in late austral winter–spring, as

well as the sign of deep convection bringing boundary layer O_3-poor air masses up to the middle–upper troposphere in late austral summer, are clearly visible in all data sets.

1 Introduction

Because of its interaction with solar and terrestrial radiation, ozone (O_3) is an important contributor to the Earth's radiative balance, and any changes in its atmospheric distribution contribute to the radiative forcing of climate change (Lacis et al., 1990). O_3 is also an important pollutant and impacts the oxidative capacity of the atmosphere (Martin et al., 2003). In the troposphere, the O_3 budget is influenced by transport from the stratosphere, by in situ photochemical production associated with O_3 precursors emitted by anthropogenic activity, biomass burning, lightning and surface deposition (Stevenson et al., 2006).

Reunion Island is a tropical island located in the southwestern part of the Indian Ocean at 20.8° S and 55.5° E. It is seasonally impacted by biomass burning plumes transported from southern Africa, South America and south-eastern Asia which can significantly affect the free tropospheric concentrations of O_3 and other pollutants like CO (Edwards et al., 2006 ; Duflot et al., 2010). Moreover, it is affected by stratospheric intrusions associated with the dynamical influence of the subtropical jet stream (Baray et al., 1998; Clain et al., 2010) and the tropical cyclone deep convection (Leclair De Bellevue et al., 2006).

The barrier effect and dynamical exchanges between the tropical reservoir and midlatitudes and vertical exchanges between the troposphere and the stratosphere, affect the O_3 balance and distribution in both the troposphere and stratosphere and are then of great interest in the documentation of climate change. Tropospheric O_3 measurements are performed routinely on Reunion Island by O_3 sondes at the Gillot site (see Fig. 1 and Table 1) since 1992 (in the framework of the Network for the Detection of Atmospheric Composition Change, NDACC, since 1996 and of the Southern Hemisphere ADditionnal OZone sondes, SHADOZ, network since 1998) and by lidar at the Université de la Réunion campus site (see Fig. 1 and Table 1) since 1998 (Baray et al., 1999, 2006).

To improve the ability of the ground-based remote sensing instruments to probe the upper-troposphere/lower-stratosphere (UT/LS) region, a high atmospheric facility was built in 2012 at the summit of the Maïdo mountain (see Fig. 1 and Table 1), and most of the instruments previously installed close to the coast at the Université de la Réunion campus site were moved up to this new facility in the year 2012 (Baray et al., 2013). Being inside the boundary layer during the day and most of the time inside the free troposphere during the night (except during the warm and rainy season), the Maïdo Observatory is dedicated to the investigation of the boundary layer composition and processes (especially in the framework of the Global Atmospheric Watch network – GAW), as well as to the study of the low–middle atmosphere (especially in the framework of the NDACC). Four lidar systems are permanently deployed and routinely operated at the Maïdo Observatory:

- a Doppler wind lidar dedicated to the study of the middle atmosphere dynamics (Khaykin et al., 2016);
- the LIO3S, a lidar dedicated to stratospheric O_3 measurements (Portafaix et al., 2003, 2016);
- the LI1200, a lidar dedicated to tropospheric water vapour (Hoareau et al., 2012; Dionisi et al., 2015; Vérèmes et al., 2017) and stratospheric-mesospheric temperature measurements (Morel et al., 2002; Keckhut et al., 2004, 2015; Sivakumar et al., 2011a);
- and the LIO3T lidar (Baray et al., 1999, 2006; Clain et al., 2009, 2010; Vérèmes et al., 2016), dedicated to the observation of tropospheric O_3 (as well as aerosols from the free troposphere up to the lower stratosphere).

It is noteworthy that the LIO3T system was very recently affiliated in the NDACC for O_3 measurements. This paper aims to provide a technical reference socle for further use of the O_3 data provided by the LIO3T system: we first present the data processing, then give a brief historical review of the tropospheric O_3 lidar system when installed at the Université de la Réunion campus site (1998–2010) together with a description of the current LIO3T system installed at the Maïdo Observatory. We show comparisons between the LIO3T O_3 measurements and O_3 external data set. We finally present an overview of the lidar tropospheric O_3 profiles database.

In the following, the system will be "LIO3T$_{UR}$" when referring to its installation at the Université de la Réunion, and the current system (installed at the Maïdo Observatory) will be referred to as "LIO3T".

2 Data processing

The programme used to calculate the O_3 profile, uncertainties and resolution is adapted from the stratospheric O_3 programme DIAL (differential absorption lidar), which has been described and intercompared by Godin et al. (1999) and is currently used for the stratospheric DIAL O_3 retrievals at Reunion Island (NDACC affiliated).

2.1 Lidar equation

The lidar DIAL technique (Hinkley, 1976) relies on the difference between two backscattered lidar signals at two different wavelengths, one where O_3 is strongly absorbed (ON, here 289 nm) and the other one where O_3 absorption is weaker (OFF, here 316 nm). The O_3 number density $n_{O_3}(z)$ at altitude z (in molec cm^{-3}) is retrieved from the Rayleigh

Table 1. Coordinates and distance to Maïdo Observatory from the observation sites used in this study.

Site	Latitude	Longitude	Altitude (m)	Distance to Maïdo (km)
Gillot	20.893° S	55.529° E	9	26
University	20.902° S	55.485° E	80	23
Maïdo Observatory	21.079° S	55.383° E	2160	0

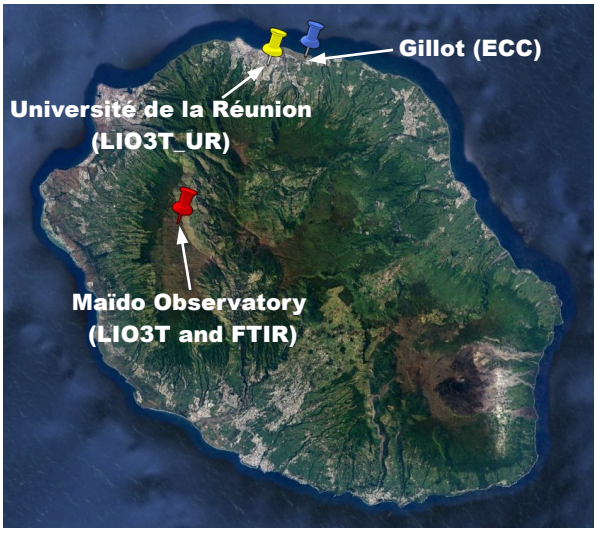

Figure 1. Map showing the locations of the different measurement sites (Maïdo Observatory, Gillot and the university on Reunion Island) and instruments ($LIO3T_{UR}$, ECC, FTIR and LIO3T) used in this study.

lidar signals according to the following equation (Harris et al., 1998):

$$n_{O_3}(z) = \frac{-1}{2\Delta\sigma_{O_3}(z)}\frac{d}{dz}\left[\ln\left(\frac{P(\lambda_{ON},z)-B(\lambda_{ON},z)}{P(\lambda_{OFF},z)-B(\lambda_{OFF},z)}\right)\right] + \delta n_{O_3}(z), \quad (1)$$

where $\Delta\sigma_{O_3}(z) = \sigma_{O_3}(\lambda_{ON},z) - \sigma_{O_3}(\lambda_{OFF},z)$ is the differential O_3 absorption cross section, $P(\lambda_i,z)$ is the number of detected photons, $B(\lambda_i,z)$ is the background noise and detector noise, and $\delta n_{O_3}(z)$ is a correction term corresponding to the absorption by other constituents of the atmosphere, expressed as follows:

$$\delta n_{O_3}(z) = \frac{1}{\Delta\sigma_{O_3}(z)}\left[\frac{1}{2}\frac{d}{dz}\left[\ln\left(\frac{\beta(\lambda_{ON},z)}{\beta(\lambda_{OFF},z)}\right)\right] - \Delta\sigma_{atm}(z)n_{atm} - \sum_{ig}\Delta\sigma_{ig}(z)n_{ig}(z)\right]. \quad (2)$$

$\beta(\lambda_i,z)$ is the coefficient of extinction of the molecules and particles, $\Delta\sigma_{atm}(z)$ and n_{atm} the differential cross section and the density of the atmosphere, respectively, and $\Delta\sigma_{ig}(z)$ and $n_{ig}(z)$ the differential cross section and the number density of interfering gas, ig, respectively. According to Leblanc et al. (2016b), the interfering gases that should be considered in practice are NO_2, SO_2 and O_2. NO_2 and SO_2 are negligible in most cases of tropospheric O_3 retrieval, except in heavy volcanic aerosols loading conditions. The absorption by O_2 should be considered if any of the detection wavelengths are shorter than 294 nm (which is the case here as we use the 289 nm wavelength). However, in our retrieval, we do not take into account any interfering gases for the time being. It is part of our plans to include them in the DIAL code. The background light, the saturation of the detector and the noise from detectors must be added to Eq. (2).

2.2 Saturation, correction and vertical resolution

The saturation is defined as the phenomenon in which the amount of output signal is no longer proportional to the incident light intensity. It is a non-linear phenomenon, depending on the dead time of the detector. In the LIO3T case, due to the detector sensitivity and the geometry of the instrument, we found that saturation occurs only below 7 km. To correct it, we apply the scheme described in Pelon (1985, Annex 2):

$$N_c = 1 + \left[\left(1 - \frac{\tau}{\delta t}\right)N_r - 1\right]e^{-\frac{\tau}{\delta t}N_r}, \quad (3)$$

with N_c the number of photons counted, N_r the number of photons received, τ the dead time of the detector and δt the integration time.

The vertical resolution is directly linked to the filtering of the lidar signal. For $LIO3T_{UR}$, the signal was filtered using a Taylor derivative filter together with a polynomial low-pass filter of the order of 2, and for LIO3T, we filter the signal with the Savitzky–Golay derivative filter of the order of 2, also called the least-squares smoothing filter (Savitzky and Golay, 1964). To take into account the decreasing signal-to-noise ratio with altitude, the number of points of the used filters (for both $LIO3T_{UR}$ and LIO3T) increases with altitude (and, consequently, the vertical resolution decreases with altitude, see Sect. 3.2 and Fig. 3). To calculate the resulting vertical resolution, the frequency approach detailed in Leblanc et al. (2016a) is used.

2.3 Uncertainty

Uncertainty calculations for DIAL O_3 retrievals are described in Leblanc et al. (2016b). The most significant

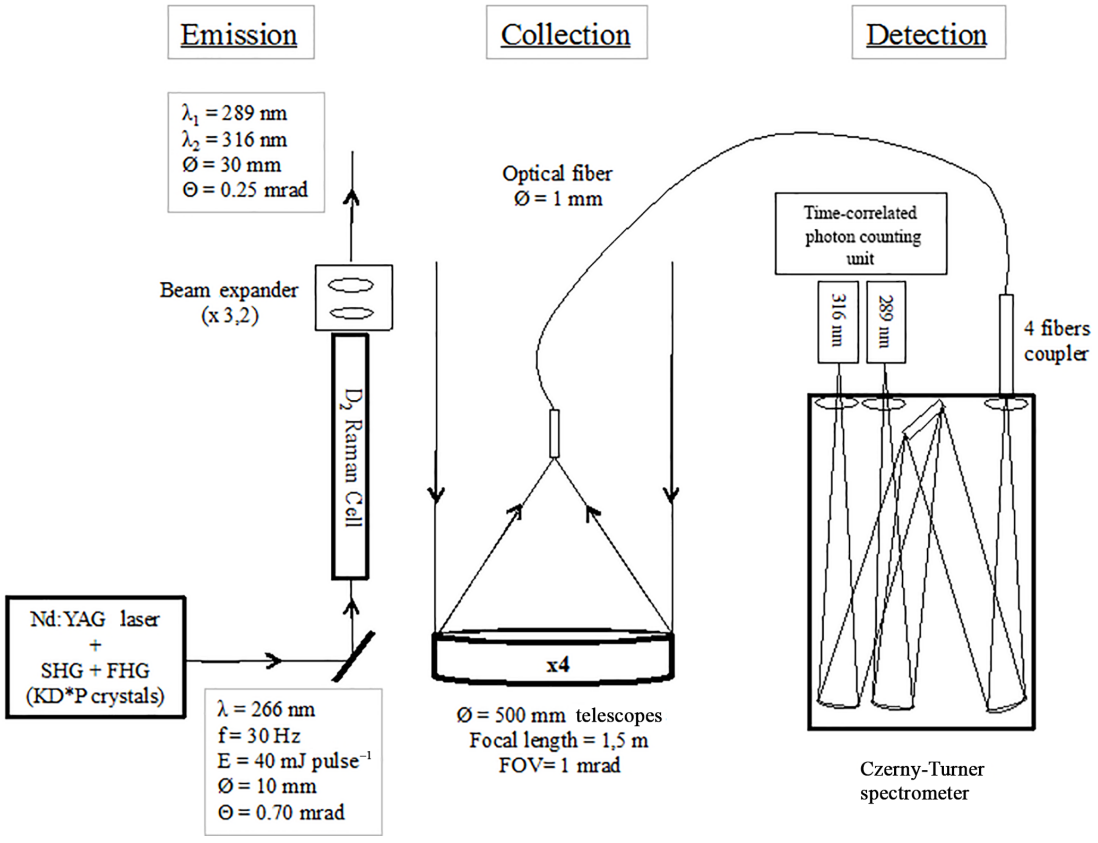

Figure 2. LIO3T instrumental schema.

sources of uncertainties are found to be the detection noise, the O_3 cross section uncertainties and the background noise.

Using our acquisition card in photon-counting mode, we calculate the detection noise by assuming that the signal's standard deviation is equal to that which is expected for a Poisson statistical distribution of detected photons. The corresponding uncertainty is thus estimated directly from the signal intensity (Leblanc et al., 2016b – Eqs. 28 and 29).

O_3 cross sections from Molina and Molina (1986) and Bass and Paur (1984) were used for O_3 profile retrievals for $LIO3T_{UR}$ and LIO3T, respectively, both with an uncertainty equal to 5 %.

The background noise includes the background light, which is altitude independent, and the detector noise – dark noise and induced signals – which are altitude dependent. We extract the background noise from the lidar signal by fitting the uppermost part of the lidar signal using a linear or polynomial regression function and by subtracting the result from the signal.

To take into account the propagation of these errors in the lidar equation, and assuming that all uncertainties are independent, we follow the approach detailed by Leblanc et al. (2016b – Eq. 4 with no covariance term).

3 Instrumental description and performance

3.1 Historical context and main instrumental features

A Rayleigh–Mie scattering lidar was first installed at the Université de la Réunion campus site in 1993 to monitor stratospheric and mesospheric aerosols in the southern tropics. From 1993 to 1998, the lidar system evolved both in terms of emission and reception (Nd:YAG laser replacement, mosaic telescopes addition, polarization channels installation, infrared channel reception set up) to improve aerosol detection and characterization and to allow stratospheric–mesospheric temperature measurement.

In 1998, an extension was installed on the existing system to perform O_3 measurements in the free troposphere, including the upper troposphere. Baray et al. (1999) give a complete description of the $LIO3T_{UR}$ and provide justifications of the technical choices that were made at this time. Note that the first "home-made" acquisition chain was exchanged for a LICEL one in 2007, but this exchange did not cause significant differences in the profiles acquired.

In late 2012, the Maïdo Observatory new facility was complete and the fixed lidar systems were moved from the Université de la Réunion campus site and installed in the Observatory. Since temperature measurements are now performed

with the LI1200 system – also dedicated to water vapour measurement (Dionisi et al., 2015; Vérèmes et al., 2017) – the previous LIO3T$_{UR}$ was modified into a system dedicated to the measurement of tropospheric O_3 (and aerosols): the LIO3T.

Figure 2 sketches the experimental schematic of the O_3 DIAL part of the LIO3T and gives its main technical characteristics. The LIO3T mainly relies on the LIO3T$_{UR}$ design (Baray et al., 1999). We use the same approach to generate a 266 nm beam going through a deuterium-filled Raman cell (using helium as buffer gas), shifting the incoming frequency to 289 and 316 nm signals. The backscattered photons are collected by the same 4×500 mm telescope mosaic focusing on 1.5 mm diameter optical fibers. Hamamatsu R9880-110 and R7400P-03 photomultiplier tubes are used for 289 and 316 nm channels, respectively. Further details on the LIO3T features can be found in Baray et al. (2013).

The detection and characterization of the tropospheric aerosols by the LIO3T is currently performed using the emitted 532 nm "residual" beam, a 200 mm telescope for reception of the elastic signal and a polarization detection system. This aerosols detection wing of the LIO3T will be the subject of dedicated studies.

3.2 Performance

The LIO3T$_{UR}$ was only operated at night to increase the signal-to-noise ratio (Kovalev and Eichinger, 2004). Due to the overlap factor (the height at which the telescope's field-of-view and laser beam overlap completely and above, where it remains constant) and detection limit, the LIO3T$_{UR}$ optimal range was 3.5–17 km above mean sea level (a.m.s.l.) (Baray et al., 1999). Note that in the following all altitudes will be given as a.m.s.l. Figures 3 and 4 give the mean vertical resolution and uncertainty profiles for LIO3T$_{UR}$ over the 13 years of operation. The temporal resolution (or integration time) depended on the atmospheric conditions (i.e. the cloud-free sky duration) and varied roughly between 40 min and 3 h. The vertical resolution varies from 0.1 km at 3 km to 1.8 km at 17 km. The mean uncertainty varies from $\approx 6\,\%$ ($\approx 3.8 \times 10^{10}$ molec cm^{-3}) at 3 km to $\approx 15\,\%$ ($\approx 7 \times 10^{10}$ molec cm^{-3}) at 16 km and increases up to 60 % ($\approx 3.5 \times 10^{11}$ molec cm^{-3}) at 17 km (not shown) where the detection noise dominates.

The altitude of the Maïdo Observatory being 2160 m, the transfer of the tropospheric O_3 DIAL system from the university (80 m) to this location increases the upper limit of the profile probed, but also increases the lower limit: the optimal range is now 6–19 km. The free troposphere, the tropical tropopause layer (TTL) and lower stratosphere are thus covered by the current system. It is worth mentioning, however, that depending on experimental conditions (lidar alignment, stability of emitted power at the transmitted wavelength, atmospheric conditions, etc.), the validity domain can vary from one day to another.

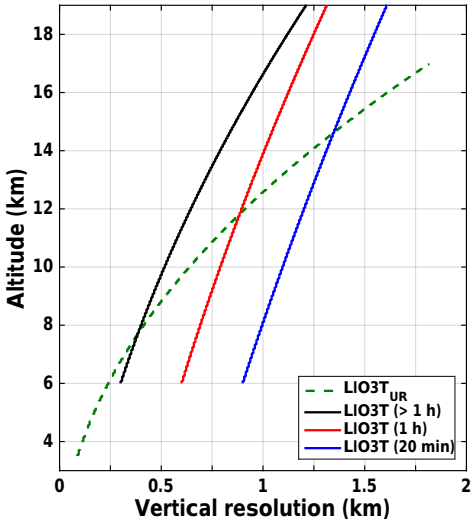

Figure 3. Mean vertical resolution of LIO3T$_{UR}$ profiles (dashed green curve) and LIO3T profiles for integration times greater than 1 h (black curve), equal to 1 h (red curve) and 20 min (blue curve).

Similarly to the LIO3T$_{UR}$, the LIO3T is only operated at night to increase the signal-to-noise ratio and twice a week in routine conditions (i.e. out of campaigns). We use three main integration times: 20 min for night-time series, 1 h for comparison with collocated ECC soundings (1 h is roughly the time for the balloon to travel the troposphere), and ≈ 3 h (between ≈ 2 and ≈ 4 h, depending on the clear-sky time duration) for full night-time profiles. Figure 3 also shows the vertical resolution resulting from each of these integration times for LIO3T. For the 20 min integration time, the resulting resolutions are 0.9 and 1.6 km at 6 and 19 km, for the 1 h integration time they are 0.7 and 1.3 km at 6 and 19 km, and for the 3 h integration time they are 0.3 and 1.2 km. The difference between the LIO3T$_{UR}$ and LIO3T vertical resolutions results from the use of different filters and numbers of points for the signal filtering (see Sect. 2.2).

Figure 4 also shows the mean uncertainties for LIO3T for the three main integration times in % (panel a) and molec cm^{-3} (panel b). Mean uncertainty varies between $\approx 7\,\%$ ($\approx 6 \times 10^{10}$ molec cm^{-3}) at 6 km and $\approx 5\,\%$ (≈ 5.5–8×10^{10} molec cm^{-3}) at 19 km with a peak at $\approx 10\,\%$ ($\approx 5 \times 10^{10}$ molec cm^{-3}), $\approx 12\,\%$ ($\approx 6 \times 10^{10}$ molec cm^{-3}) and $\approx 15\,\%$ ($\approx 7.5 \times 10^{10}$ molec cm^{-3}) at 16 km for the >1 h, 1 h and 20 min integration times, respectively. These figures are in agreement with the recently published work of Leblanc et al. (2016b), showing uncertainty profiles for a 2 h DIAL tropospheric O_3 measurement between 7 and 11 %. One can notice that, above 16 km, the LIO3T$_{UR}$ uncertainty increases and is greater than the LIO3T one. By contrast, the LIO3T uncertainty decreases (in %) between 16 and 19 km. This can be explained by the fact that LIO3T$_{UR}$ reaches its detection limit between ≈ 16 and ≈ 17 km (where the detection noise dominates), while for LIO3T the increase in the

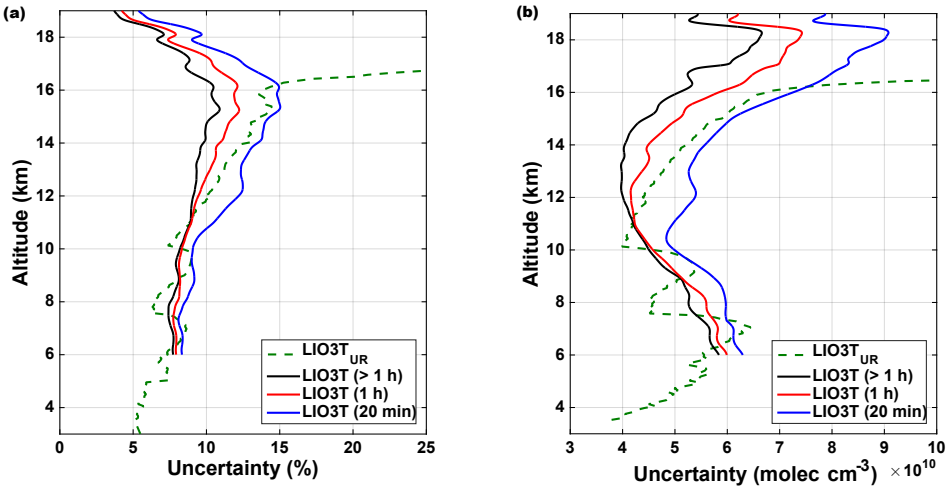

Figure 4. Mean uncertainties in % **(a)** and molec cm^{-3} **(b)** of the LIO3T$_{UR}$ profiles (dashed green curve) and LIO3T profiles for integration times greater than 1 h (black curve), equal to 1 h (red curve) and equal to 20 min (blue curve).

detection noise is balanced by the increase of the O_3 abundance when entering the stratosphere.

The main benefit of the instrument altitude change from 80 to 2160 m is that it enables the UT/LS region to be documented with relevant vertical and time resolutions together with a reasonable uncertainty (1.5 km, 20 min and 10 % at 18 km).

4 Comparisons of LIO3T measurements with O_3 external data set

The goal of this section is to validate the LIO3T O_3 measurements by comparing them to the O_3 external data set. Four types of correlative data are used here: eight collocated ECC soundings (i.e. launched from the Maïdo Observatory during a lidar shooting), 37 routine NDACC/SHADOZ ECC soundings performed during the daytime at the Gillot site (see Fig. 1 and Table 1), and Fourier transform infrared spectrometer (FTIR) tropospheric partial columns measurements from both daytime ground-based (12 comparison pairs) and nighttime Infrared Atmospheric Sounding Interferometer (IASI) (39 comparison pairs) data.

In the following, we compare N LIO3T O_3 measurements M_{LIO3T} with N correlative data M_{CD} by calculating the mean absolute relative difference between data sets D (in %) defined as follows:

$$D = \frac{1}{N}\sum_{n=1}^{N}|r_n|, \tag{4}$$

with r_n the relative difference (in %) between two observations M_{LIO3T_n} and M_{CD_n} defined as follows:

$$r_n = 100 \cdot \frac{M_{\mathrm{LIO3T}_n} - M_{\mathrm{CD}_n}}{\frac{M_{\mathrm{LIO3T}_n} + M_{\mathrm{CD}_n}}{2}}. \tag{5}$$

4.1 Comparison with ECC

ECC sondes measure the oxidation of a potassium iodine (KI) solution by O_3 (Komhyr et al., 1995). Their precision is 5–10 % throughout the troposphere and TTL (Smit et al., 2007) and they are commonly used for the validation of ground-based and space-borne O_3 observations. Here below, we compare LIO3T O_3 profiles with both collocated Maïdo ECC soundings and Gillot SHADOZ/NDACC routine daytime ECC soundings. All these ECC profiles are generated following the "Guidelines for homogenization of ozonesonde data" (Smit et al., 2012). The Gillot SHADOZ/NDACC reprocessed ECC data set was recently presented by Posny et al. (2016) and Witte et al. (2017) and is used in this article. Moreover, similar reprocessing was applied to the ECC soundings performed at the Maïdo Observatory. From August 2007 to December 2016, ECC soundings were performed at Reunion Island using the ENSCI/0.5 % full buffer solution instead of the standard half buffer. This specificity of the Reunion Island ECC soundings is not taken into account in the SHADOZ/NDACC reprocessed ECC data set yet. Following the work of Johnson et al. (2002, 2016), who intercompared various KI and buffer solutions, we found that this ENSCI/0.5 % full buffer solution tends to overestimate the amount of O_3 by 1.7 % on average in the troposphere. Consequently, an adapted correction was applied to the ECC profiles acquired during this period.

Figure 5 shows the comparison between LIO3T and eight ECC soundings collocated in time and space: two were performed in June 2013, four in May 2015 and two in July 2015. Note that these last six were part of the Maïdo ObservatoRy Gaz and Aerosols Ndacc Experiment (MORGANE) campaign that took place in May–July 2015 (Portafaix et al., 2016; Duflot et al., 2016; Posny et al., 2016; Vérèmes et al., 2017). The integration time for the LIO3T profiles

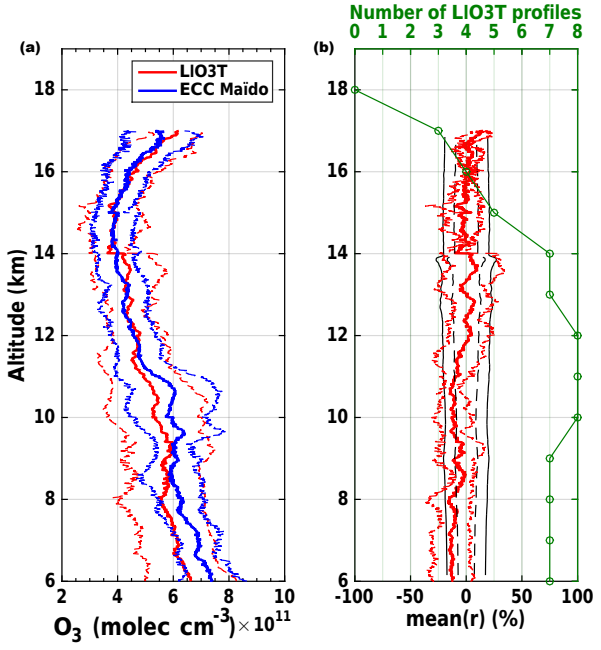

Figure 5. (a) Mean LIO3T O_3 profile (red curve) and mean ECC profile (blue curve) measured during the eight intercomparison measurements performed at Maïdo. The dashed lines give the 1 standard deviation around the mean. **(b)** Mean r between the LIO3T and ECC profiles (red curve), mean LIO3T uncertainty around zero (black dashed lines) and mean LIO3T uncertainty and ECC precision around zero (black lines). The red dashed lines give the 1 standard deviation around the r mean. The green line (upper x axis) gives the number of LIO3T profiles used for comparison.

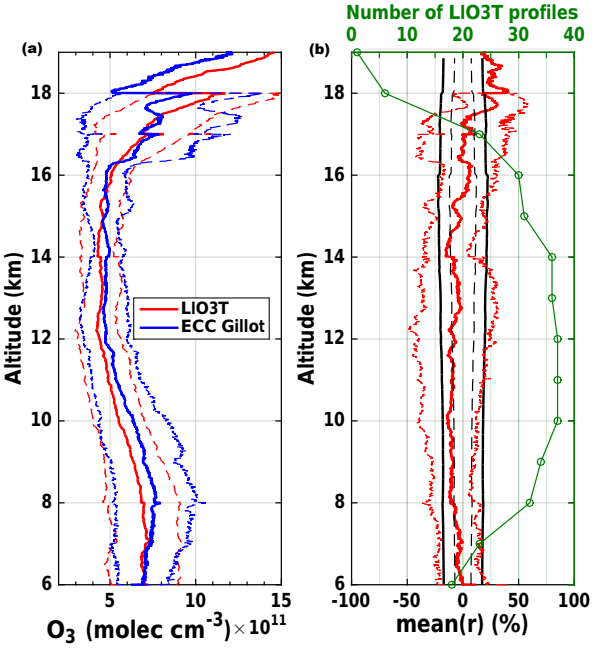

Figure 6. Same as Fig. 5 for NDACC/SHADOZ Gillot ECC soundings and full night-time LIO3T profiles.

used here is 1 h (starting at the ECC sonde launch time) and corresponds roughly to the time for the balloon to travel the troposphere. Note that the discontinuities in the mean profiles shown on Fig. 8 are caused by the varying valid ranges in the LIO3T profiles (see Table 2), and note that no profile goes above 17 km for these eight comparisons. In particular, the valid range in May and July 2015 (during the MORGANE campaign) is bounded up at 17 km by the volcanic aerosol loading coming from the Calbuco volcano (Chile, 41.32° S, 72.62° W), which erupted late April 2015 and whose volcanic plume reached the TTL above Reunion Island on the 6 May 2015 before slowly vanishing near the end of July 2015 (Bègue et al., 2017). This aerosol enhancement is clearly visible on the 355 nm channels of the stratospheric O_3 and LI1200 lidars and on the 532 nm channel of the LIO3T (not shown), and back trajectories together with CALIOP observations (on board CALIPSO – not shown) show that the detected plume comes from the Calbuco volcano (Bègue et al., 2017). Consequently, although we do not have any information on the corresponding aerosol and SO_2 amount, we consider it wise to assume that, in the layer where this volcanic plume lies (i.e. between 17 and 22 km), the SO_2 and aerosols loading is too strong to allow a correct O_3 retrieval (Ancellet et al., 1987; McGee et al., 1993).

One can see on Fig. 5 that there is an overall agreement between LIO3T and the ECC considering the lidar uncertainty and ECC precision (panel b). D is 6.8 % for the whole probed column (LIO3T lower than ECC). This value agrees with the ones recently reported for single or multiple ECC-lidar comparisons (between 6 and 20 % reported by Uchino et al., 2014; 20 % reported by Sullivan et al., 2015; 8 % reported by Gaudel et al., 2015).

Figure 6 shows the comparison between the SHADOZ/NDACC Gillot routine ECC soundings and LIO3T profiles. As the first ones are performed during the daytime (usually around 15:00:00 LT) and the last ones during night-time (between 19:00:00 and 01:00:00 LT), ECC soundings are taken into consideration when performed 1 day before or after a LIO3T profile acquisition; we find 37 pairs for comparison over the years 2013–2015. The LIO3T profiles used here are full night-time profiles. Once again, note that the discontinuities in the mean profiles shown on Fig. 6 are caused by the varying valid ranges in the LIO3T profiles (and one can see that only one profile is above 18 km). Despite the fact that the instruments were neither collocated in time nor space (the ECC launch site – Gillot – is 26 km away from the Maïdo Observatory (see Table 1) and balloons are advected by the wind), one can see that there is an overall good agreement between measurements considering the lidar uncertainty and ECC precision, with a mean D equal to 9.4 % over the entire 6–19 km column (LIO3T lower than ECC).

Table 2. Dates of comparisons with collocated ECC soundings and corresponding LIO3T O_3 profile valid ranges. Italicized dates indicate profiles impacted by the Calbuco eruption.

Date	Profile valid range (km)
2013/06/24	6–14
2013/06/25	6–14
2015/05/11	6–17
2015/05/15	10–16
2015/05/26	6–12
2015/05/28	6–17
2015/07/06	6–15
2015/07/07	6–17

4.2 Comparison with ground-based and space-borne FTIRs

In this section we compare the LIO3T profiles with collocated partial column measurements performed by two FTIRs: the Bruker 125HR installed at the Maïdo Observatory since 2013 and IASI on board the MetOp-A satellite.

4.2.1 Comparison with NDACC ground-based FTIR measurements

A Bruker 125HR FTIR spectrometer started operating at the Maïdo Observatory in March 2013 with a primary dedication to NDACC measurements (Zhou et al., 2016). This NDACC ground-based FTIR observes the absorption of the direct solar radiation with high spectral resolution (0.0035–0.0110 cm^{-1}) and uses the pressure-broadening effect of absorption lines to retrieve volume mixing ratio (vmr) low vertical resolution profiles of target gases. The FTIR O_3 measurements show good sensitivity from the ground up to about 45 km. Within this vertical range, about four vertical layers can be distinguished; i.e. the vertical resolution varies from 8 to 15 km (Vigouroux et al., 2015). In this study, the FTIR retrievals are based on an optimal estimation method (Rodgers, 2000) carried out with the SFIT4 algorithm (https://wiki.ucar.edu/display/sfit4), which is an open source code, jointly developed at the NASA Langley Research Center, the National Center for Atmospheric Research (NCAR), the National Institute of Water and Atmosphere Research (NIWA) and the University of Bremen. HBr cell measurements are performed on a daily basis to verify the alignment of the instrument and to obtain the instrument line shape (ILS) using the LINEFIT14.5 programme (Hase et al., 1999). The retrieval scheme is described in Vigouroux et al. (2015) and closely follows the recipe of the Jungfraujoch station (except for the ILS which is fixed from LINEFIT results at Maïdo): the retrieval microwindow is 1000–1005 cm^{-1}, the a priori data come from the WACCMv6 model and pressure and temperature a priori profiles were obtained from the National

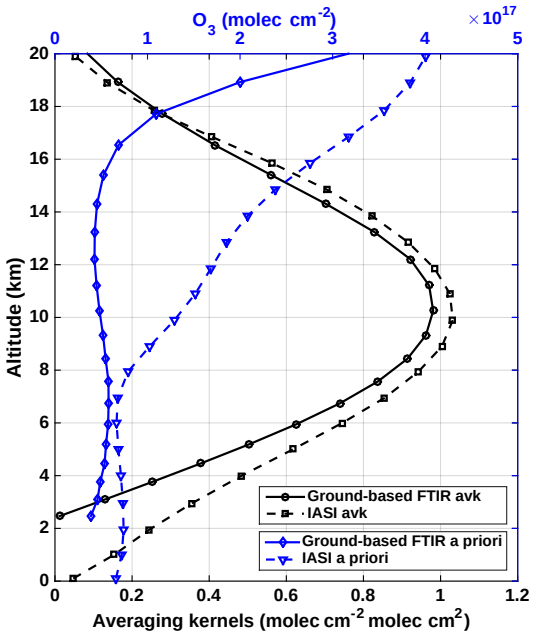

Figure 7. Lower x axis: ground-based NDACC FTIR (black curve and circles) and IASI (black dashed curve and squares) averaging kernels for the 8–16 and 6–16 km partial columns, respectively. Upper x axis: ground-based NDACC FTIR (blue curve and diamonds) and IASI (blue dashed curve and triangles) O_3 a priori profiles.

Centers for Environmental Prediction. The a priori water profile is obtained from a dedicated pre-retrieval. Each O_3 profile is retrieved with the signal to noise of the source spectrum. The total uncertainty of the O_3 profile is dominated by the smoothing error (i.e. the poor vertical resolution of the profile), the temperature and the spectroscopic uncertainties. We use the following approach for comparison:

i. FTIR observations were performed during the daytime. Each LIO3T measurement is compared to all FTIR measurements within a 24 h time window.

ii. For each pair (114 pairs in total), the LIO3T profile is regridded consistently with the FTIR.

iii. FTIR measurements are averaged within the 24 h time window around a single LIO3T measurement for comparison.

iv. At this stage we have a set of comparable pairs of measurements with various validity domains for LIO3T profiles; however, the method needs constant boundaries for the partial column used for comparison. We then choose the partial column shared by a sufficient number of LIO3T profiles to allow a reasonable comparison. The upper and lower limits of this partial column are hereafter called "valid range for comparison".

v. The regridded LIO3T profile is smoothed with the FTIR averaging kernel matrix and a priori (see e.g. Rodgers

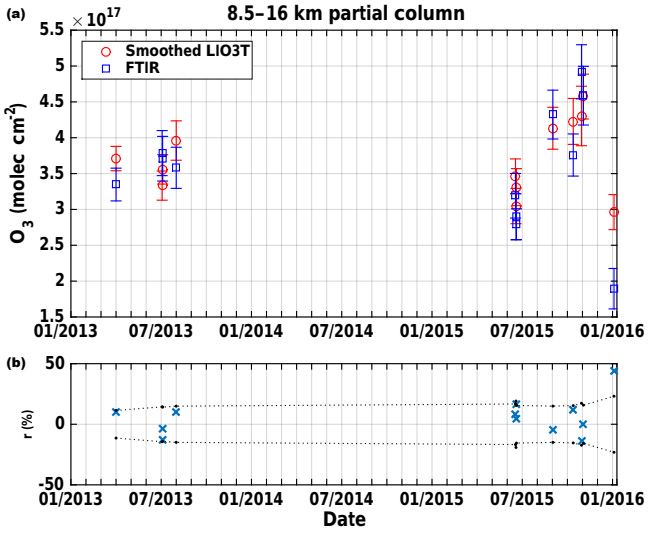

Figure 8. (a) Smoothed LIO3T (red circles) and ground-based NDACC FTIR (blue squares) 8.5–16 km O_3 partial columns. Vertical bars give uncertainties for each measurement. **(b)** r (%) between LIO3T and FTIR measurements (blue crosses) superimposed on LIO3T + FTIR uncertainties around zero (black dotted lines and dots).

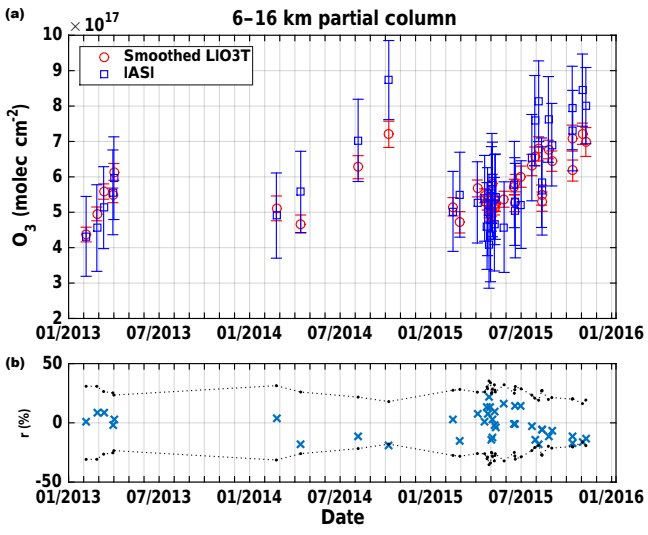

Figure 9. (a) Smoothed LIO3T (red circles) and IASI (blue squares) 6–16 km O_3 partial columns. Vertical bars give uncertainties for each measurement. **(b)** r (%) between LIO3T and IASI measurements (blue crosses) superimposed on LIO3T + IASI uncertainties around zero (black dotted lines and dots).

and Connor, 2003; Vigouroux et al., 2008). To allow for smoothing, the LIO3T measured profiles are extended by the FTIR a priori outside the valid range for comparison. By smoothing the LIO3T profiles, we degrade them to the FTIR low vertical resolution, and we can get rid of the FTIR smoothing uncertainty associated with the comparison.

vi. Finally, a partial column is calculated from this smoothed LIO3T profile in the valid range of comparison.

We find 12 comparison pairs over the studied period within the 8.5–16 km valid range for comparison. In this 8.5–16 km partial column, the ground-based NDACC FTIR has 1.1 degree of freedom (Rodgers, 2000) and a mean total uncertainty of 7.5 %. Figure 7 shows the FTIR a priori profile and averaging kernels for this 8.5–16 km partial column, both of which are used to smooth the LIO3T measurements to compare them with the FTIR ones.

Figures 8 shows the comparison of the FTIR and LIO3T partial columns available over the January 2013–January 2016 period. One can see that there is good agreement between the data sets, taking into account the uncertainties. We find a D of 11.8 % between data sets (LIO3T higher than FTIR). Note that, due to the sparse comparison points, the Southern Hemisphere biomass burning season is not visible on this plot.

4.2.2 Comparison with IASI measurements

IASI is on board the MetOp-A satellite, launched in a Sun-synchronous orbit around the Earth at the end of 2006. A second IASI was launched on board MetOp-B in September 2012 and the launch of the third one (MetOp-C) is planned for late 2018. In this comparison, IASI/MetOp-A data are used. IASI is a FTIR instrument that measures the thermal infrared radiation emitted by the Earth's surface and atmosphere in the 645–2760 cm^{-1} spectral range with a spectral resolution of 0.5 cm^{-1} apodized and a radiometric noise below 0.2 K between 645 and 950 cm^{-1} at 280 K (Clerbaux et al., 2009).

IASI is an interesting instrument for our intercomparison effort as it provides global Earth coverage twice daily with overpass times at 09:30:00 and 21:30:00 mean local time and a nadir footprint on the ground of 12 km. IASI has significant sensitivity to tropospheric O_3. As LIO3T usually fires between 19:00:00 and 01:00:00 local times, here we used the IASI night-time overpass measurements. The IASI data used in this study come from the FORLI-O_3 v20151001 scheme (Hurtmans et al., 2012; Boynard et al., 2016).

To compare measurements from both instruments, IASI retrievals are averaged over a 1° × 1° box around the Maïdo Observatory location. We then use the same approach as described in Sect. 4.2.1 (except points i and iii). We find 39 comparison pairs over the studied period within the 6–16 km valid range for comparison. In this 6–16 km partial column, IASI has 1.6 degree of freedom (Rodgers, 2000) and a mean total uncertainty equal to 18.4 %. Figure 7 shows the mean IASI a priori profile and mean averaging kernels in the 6–

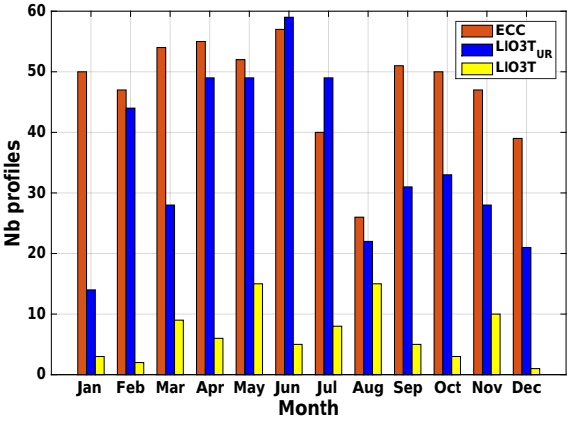

Figure 10. Number of O_3 profiles per month for ECC (1998–2015, 568 profiles), LIO3T$_{UR}$ (1998–2010, 427 profiles) and LIO3T (January 2013–January 2016, 84 profiles).

16 km partial column for the 39 comparison pairs. In the following, LIO3T measurements are smoothed according to the characteristics of the IASI retrievals.

Figure 9 shows the comparison of the IASI and LIO3T partial column time series. We obtain a good agreement between the data sets considering the uncertainties. We find a D of 11.3 % between data sets (LIO3T higher than IASI). These results are in agreement with the 5–15 % O_3 abundance difference of IASI in the troposphere compared to ECC soundings reported recently by Boynard et al. (2016). Note that, due to the sparse comparison points, the Southern Hemisphere biomass burning season is barely visible on this plot.

5 Data set and climatologies

Figure 10 shows the monthly distribution of the number of O_3 profiles acquired by the NDACC/SHADOZ ECC (Gillot, 1998–2015, 568 profiles), LIO3T$_{UR}$ (Université de la Réunion, 1998–2010, 427 profiles), and LIO3T (Maïdo Observatory, 2013–2015, 84 profiles). The low number of lidar profiles in the austral summer period (especially December–January) is explained by the high occurrence of cloudy skies. In particular, one can see that only one LIO3T profile is available for December (which ends up at 10 km due to a misalignment of the LIO3T). The lower limit of LIO3T profiles range from 6 to 10 km and the upper limit ranges from 12 to 19 km. Most LIO3T profiles start at 6 km and end at 17–18 km.

Figure 11 shows the three resulting monthly tropospheric O_3 climatologies, on which the following seasonal features can be observed:

- A clear increase of O_3 abundance is seen over the whole tropospheric column – especially between 2 and 10 km – starting in June and ending in December with a maximum in October of $\approx 10 \times 10^{11}$ molec cm^{-3} on average between 4 and 10 km. This increase is due to the influence of air masses coming from South America, southern Africa and south-eastern Asia (Edwards et al., 2006; Duflot et al., 2010), where the biomass burning season occurs every year during this period. O_3 abundance then presents a slow decay over the entire tropospheric column from January to May.
- There is a decrease of the ozonopause altitude from ≈ 17 km in December–July down to ≈ 15 km in August–November (Sivakumar et al., 2011b), which is likely a combination of the spring and summer maximum of occurrence of stratosphere-to-troposphere exchanges (STE) above Reunion Island (Clain et al., 2010) and of the wintertime thermal effect on the troposphere thickness.
- The minimum of O_3 abundance occurs in February between 10 and 16 km ($\approx 3 \times 10^{11}$ molec cm^{-3} on average), which is likely a sign of the austral summer deep convection bringing boundary layer O_3-poor air masses up to the middle–upper troposphere.

In conclusion, the three data sets show a remarkable – and reassuring – agreement in terms of patterns and values.

Figure 12 shows the seasonal profiles derived from the LIO3T measurements. The Southern Hemisphere biomass burning season is still clearly visible in the September–October–November profile (SON), with an increase that covers the whole of the probed column, and also on the June–July–August (JJA) profile from 6 to 13 km.

6 Conclusions and future plans

A DIAL tropospheric O_3 lidar was operating on the Université de la Réunion campus site from 1998 to 2010, providing 427 O_3 profiles. In 2012, the system was moved up to the Maïdo Observatory and routine O_3 observations started in February 2013 by the LIO3T. From then until January 2016, 84 O_3 profiles were acquired and the LIO3T operation is ongoing. These O_3 measurements were recently affiliated in the NDACC.

The LIO3T observation scheme is based on the DIAL technique, which currently detects two wavelengths, 289 and 316 nm, with multiple receivers. The transmitted wavelengths are generated by focusing the output of a quadrupled Nd:YAG laser beam (266 nm) onto a Raman cell filled with high-pressure deuterium, using helium as buffer gas. With knowledge of the O_3 absorption coefficient at these two wavelengths, the range-resolved number density can be derived.

The optimal range for the actual system is 6–19 km, depending on the system performance and atmospheric conditions. For a 1 h integration time, vertical resolution varies from 0.7 km at 6 km to 1.3 km at 19 km, and mean uncertainty over the 6–19 km range is between ≈ 6 and ≈ 13 %.

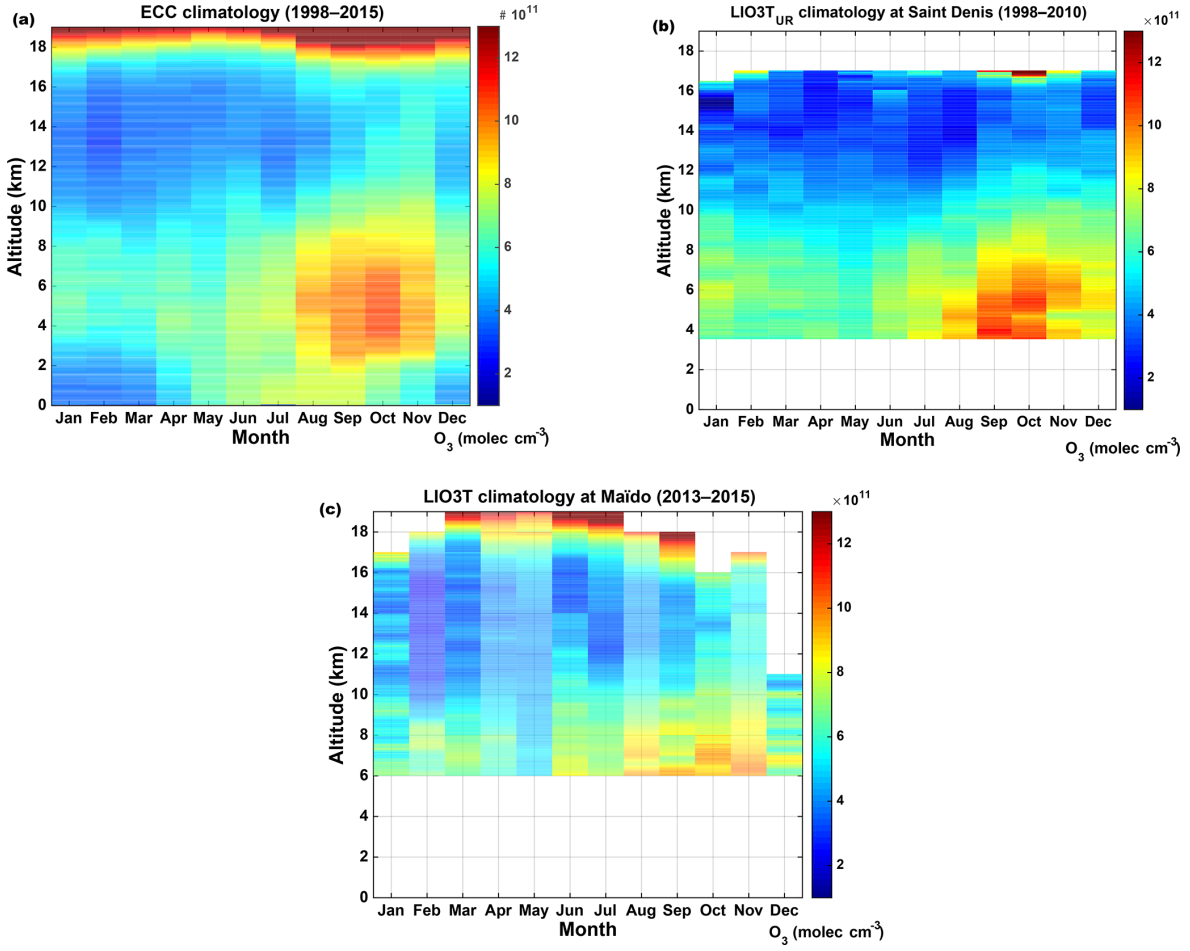

Figure 11. Monthly O_3 climatology between 0 and 19 km derived from ECC sondes over 1998–2015 at the Gillot site **(a)**, from LIO3T$_{UR}$ over 1998–2010 at Université de la Réunion campus site **(b)** and from LIO3T over 2013–2015 at Maïdo Observatory (including data routinely performed and from intensive period of observations) **(c)**.

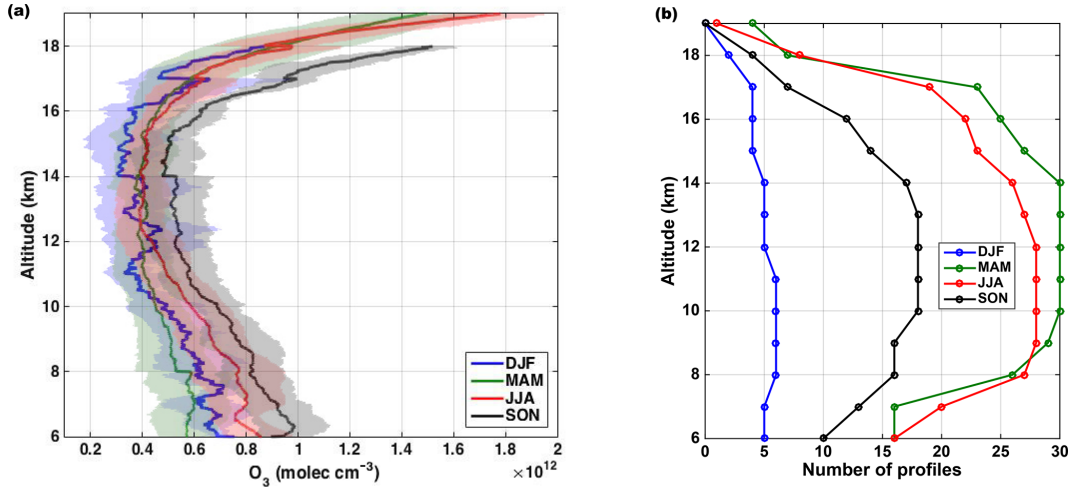

Figure 12. (a) Seasonal LIO3T O_3 profiles for DJF (blue curve – 8 profiles), MAM (green curve –30 profiles), JJA (red curve – 25 profiles) and SON (black curve – 21 profiles). The shaded areas give the 1 standard deviation around the mean. **(b)** Number of LIO3T profiles used for each climatological profile.

Comparisons with O_3 external data set were performed showing good agreement between data sets considering the uncertainties: we found a 6.8 % D between LIO3T observations and eight ECC sondes simultaneously launched from the Maïdo Observatory (LIO3T lower than ECC), 9.4 % D between LIO3T observations and 37 ECC sondes launched from the Gillot site during the daytime in a ±24 h window around lidar shooting (LIO3T lower than ECC), 11.8 % D between LIO3T and 12 ground-based NDACC FTIR measurements acquired during the daytime in a ±24 h window around lidar shooting in the 8.5–16 km partial column (LIO3T higher than FTIR), and 11.3 % D between LIO3T and 39 simultaneous night-time IASI observations over Reunion Island in the 6–16 km partial column (LIO3T higher than IASI).

ECC, $LIO3T_{UR}$ and LIO3T monthly climatologies all exhibit the same range of values and the same seasonal patterns:

- the O_3 abundance increase between 6 and 10 km in austral winter and spring due to the Southern Hemisphere biomass burning season;
- the ozonopause altitude decrease from ≈ 17 to ≈ 15 km from late austral winter to early austral summer due to the wintertime thermal effect on the troposphere thickness combined with the enhanced occurrence of STE in austral spring and summer;
- the O_3 abundance minimum between 10 and 16 km in late austral summer in the middle–upper troposphere due to deep convection uplifting O_3-poor air masses from the boundary layer.

Moving this lidar from the Université de la Réunion campus site up to the Maïdo observatory allows it to document the UT/LS region and to follow stratospheric and tropospheric intrusions with relevant vertical and time resolutions together with a reasonable uncertainty (1.5 km, 20 min and 10 %, respectively, at 18 km). This tropospheric O_3 data set covering the tropical free troposphere and UT/LS of a sparsely documented region (south-western Indian Ocean) constitutes an extremely valuable resource for the validation of satellite tropospheric O_3 retrievals, analysis of the O_3 variability and sources, dynamics analysis of case studies and for long-term atmospheric monitoring.

Future plans for the LIO3T are to (1) use the available 532 nm residual beam to detect and study aerosols in the free troposphere, TTL and lower stratosphere. The use of the infrared signal (1064 nm) to study aerosols is also planned. (2) NDACC recommendations will be implemented in the data processing (O_3 cross sections, background and saturation corrections uncertainties propagation, interfering gases). (3) Uncertainties will be calculated due to the presence of aerosols in the troposphere using an iterative aerosol assessment procedure, ideally using the 532 nm backscattered signal.

Data availability. LIO3T system was very recently affiliated in the NDACC for O3 measurements. The LIO3T data used in this article will be soon available in the NDACC database, accessible at http://www.ndsc.ncep.noaa.gov/ (Network for the Detection of Atmospheric Composition Change, 2017). The IASI L1C data and L2 temperature data used in this study are currently not publicly available. These data were provided by the Aeris data infrastructure (AERIS, 2017).

Competing interests. The authors declare that they have no conflict of interest.

Special issue statement. This article is part of the special issue "Twenty-five years of operations of the Network for the Detection of Atmospheric Composition Change (NDACC) (AMT/ACP/ESSD inter-journal SI)". It is not associated with a conference.

Acknowledgements. The authors acknowledge the European Communities, the Région Réunion, CNRS, and Université de la Réunion for their support and contributions in the construction phase of the research infrastructure OPAR (Observatoire de Physique de l'Atmosphère de La Réunion). OPAR is presently funded by CNRS (INSU) and Université de La Réunion and managed by OSU-R (Observatoire des Sciences de l'Univers de La Réunion, UMS 3365). The authors also gratefully acknowledge Eric Golubic, Patrick Hernandez and Louis Mottet, who are deeply involved in the routine lidar observations at the Maïdo facility. Jacquelyn Cecile Witte (NASA/GSFC) is acknowledged for the ECC data reprocessing. IASI is a joint mission of EUMETSAT and the Centre National d'Etudes Spatiales (CNES, France). The IASI L1C data are distributed in near real time by EUMETSAT through the EUMETCast system distribution. The authors acknowledge the Aeris data infrastructure for providing access to the IASI L1C data and L2 temperature data used in this study (available at: http://www.aeris-data.fr/?locale=en). This work was undertaken in the framework of the EUMETSAT O_3M-SAF project (http://acsaf.org/), the European Space Agency O_3 Climate Change Initiative (O_3-CCI, http://www.esa-ozone-cci.org). The ULB French scientists are grateful to CNES and Centre National de la Recherche Scientifique (CNRS) for financial support. PFC is grateful to Belspo and ESA (Prodex IASI.Flow project) for financial support. The colleagues from BIRA-IASB acknowledge the support from the Belgian Science Policy Office, as well as from ESA/PRODEX and the Copernicus programme (CAMS-VAL).

Edited by: Gabriele Stiller
Reviewed by: three anonymous referees

References

AERIS: AERIS data and services, CNRS/CNES/Météo France/Université Lille 1/Région Nord-Pas-de-Calais/Université Paul Sabatier/Université Pierre et Marie Curie/CEA/École Polytechnique/IGN/IRD, Institut Pierre Simon Laplace, Quartier des Garennes, 11 Bouvelard d'Alembert, 78280 Guyancourt, France,

available at http://www.aeris-data.fr, last access: 13 September 2017.

Ancellet, G., Mégie, G., Pelon, J., Capitini, R., and Renaut, D.: Lidar measurements of sulfur dioxide and ozone in the boundary layer during the 1983 Fos Berre Campaign, Atmos. Environ., 21, 2215–2226, 1987.

Baray, J.-L., Ancellet, G., Taupin, F. G., Bessafi, M., Baldy, S., and Keckhut, P.: Subtropical tropopause break as a possible stratospheric source of ozone in the tropical troposphere, J. Atmos. Sol.-Terr. Phy., 60, 27–36, 1998.

Baray, J.-L., Leveau, J., Porteneuve, J., Ancellet, G., Keckhut, P., Posny, F., and Baldy, S.: Description and evaluation of a tropospheric ozone lidar implemented on existing lidar in the southern tropics, Appl. Optics, 38, 6808–6817, 1999.

Baray, J. L., Leveau, J., Baldy, S., Jouzel, J., Keckhut, P., Bergametti, G., Ancellet, G., Bencherif, H., Cadet, B., Carleer, M., David, C., De Mazière, M., Faduilhe, D., Godin-Beekmann, S., Goloub, P., Goutail, F., Metzger, J. M., Morel, B., Pommereau, J. P., Porteneuve, J., Portafaix, T., Posny, F., Robert, L., and Van Roozendael, M.: An instrumented station for the survey of ozone and climate change in the southern tropics: Scientific motivation, technical description and future plans, J. Environ. Monitor., 8, 1020–1028, https://doi.org/10.1039/b607762e, 2006.

Baray, J.-L., Courcoux, Y., Keckhut, P., Portafaix, T., Tulet, P., Cammas, J.-P., Hauchecorne, A., Godin Beekmann, S., De Mazière, M., Hermans, C., Desmet, F., Sellegri, K., Colomb, A., Ramonet, M., Sciare, J., Vuillemin, C., Hoareau, C., Dionisi, D., Duflot, V., Vérèmes, H., Porteneuve, J., Gabarrot, F., Gaudo, T., Metzger, J.-M., Payen, G., Leclair de Bellevue, J., Barthe, C., Posny, F., Ricaud, P., Abchiche, A., and Delmas, R.: Maïdo observatory: a new high-altitude station facility at Reunion Island (21° S, 55° E) for long-term atmospheric remote sensing and in situ measurements, Atmos. Meas. Tech., 6, 2865–2877, https://doi.org/10.5194/amt-6-2865-2013, 2013.

Bass, A. M. and Paur, R. J.: The ultraviolet cross-sections of ozone: I: The measurements, II: Results and temperature dependence, Ozone Symposium, Greece, 1984.

Bègue, N., Vignelles, D., Berthet, G., Portafaix, T., Payen, G., Jégou, F., Benchérif, H., Jumelet, J., Vernier, J.-P., Lurton, T., Renard, J.-B., Clarisse, L., Duverger, V., Posny, F., Metzger, J.-M., and Godin-Beekmann, S.: Long-range isentropic transport of stratospheric aerosols over Southern Hemisphere following the Calbuco eruption in April 2015, Atmos. Chem. Phys. Discuss., https://doi.org/10.5194/acp-2017-544, in review, 2017.

Boynard, A., Hurtmans, D., Koukouli, M. E., Goutail, F., Bureau, J., Safieddine, S., Lerot, C., Hadji-Lazaro, J., Wespes, C., Pommereau, J.-P., Pazmino, A., Zyrichidou, I., Balis, D., Barbe, A., Mikhailenko, S. N., Loyola, D., Valks, P., Van Roozendael, M., Coheur, P.-F., and Clerbaux, C.: Seven years of IASI ozone retrievals from FORLI: validation with independent total column and vertical profile measurements, Atmos. Meas. Tech., 9, 4327–4353, https://doi.org/10.5194/amt-9-4327-2016, 2016.

Clain, G., Baray, J. L., Delmas, R., Diab, R., Leclair de Bellevue, J., Keckhut, P., Posny, F., Metzger, J. M., and Cammas, J. P.: Tropospheric ozone climatology at two Southern Hemisphere tropical/subtropical sites, (Reunion Island and Irene, South Africa) from ozonesondes, LIDAR, and in situ aircraft measurements, Atmos. Chem. Phys., 9, 1723–1734, https://doi.org/10.5194/acp-9-1723-2009, 2009.

Clain, G., Baray, J.-L., Delmas, R., Keckhut, P., and Cammas, J.-P.: A Lagrangian approach to analyse the tropospheric ozone climatology in the tropics: Climatology of stratosphere-troposphere exchange at Reunion Island, Atmos. Environ., 44, 968–975, 2010.

Clerbaux, C., Boynard, A., Clarisse, L., George, M., Hadji-Lazaro, J., Herbin, H., Hurtmans, D., Pommier, M., Razavi, A., Turquety, S., Wespes, C., and Coheur, P.-F.: Monitoring of atmospheric composition using the thermal infrared IASI/MetOp sounder, Atmos. Chem. Phys., 9, 6041–6054, https://doi.org/10.5194/acp-9-6041-2009, 2009.

Dionisi, D., Keckhut, P., Courcoux, Y., Hauchecorne, A., Porteneuve, J., Baray, J. L., Leclair de Bellevue, J., Vérèmes, H., Gabarrot, F., Payen, G., Decoupes, R., and Cammas, J. P.: Water vapor observations up to the lower stratosphere through the Raman lidar during the Maïdo Lidar Calibration Campaign, Atmos. Meas. Tech., 8, 1425–1445, https://doi.org/10.5194/amt-8-1425-2015, 2015.

Duflot, V., Dils, B., Baray, J.-L., De Mazière, M., Attié, J.-L., Vanhaelewyn, G., Senten, C., Vigouroux, C., Clain, G., and Delmas, R.: Analysis of the origin of the distribution of CO in the subtropical southern Indian Ocean in 2007, J. Geophys. Res.-Atmos., 115, D22106, https://doi.org/10.1029/2010JD013994, 2010.

Duflot, V., Payen, G., Marquestaut, N., Vérèmes, H., Portafaix, T., Posny, F., Keckhut, P., Hauchecorne, A., Khaykin, S., Godin-Beekman, S., Leblanc, T., McGee, T., Sumnicht, G., Evan, S., Brioude, J., Bègue, N., Vernier, J.-P., Dirksen, R., Vömel, H., and Cammas, J.-P.: Reunion Island NDACC Lidars Operations 2013–2016 and the MORGANE campaign, NDACC Lidar Working Group, Payerne, Switzerland, 2016.

Edwards, D. P., Emmons, L. K., Gille, J. C., Chu, A., Attié, J.-L., Giglio, L., Wood, S. W., Haywood, J., Deeter, M. N., Massie, S. T., Ziskin, D. C., and Drummond, J. R.: Satellite-observed pollution from Southern Hemisphere biomass burning, J. Geophys. Res.-Atmos., 111, D14312, https://doi.org/10.1029/2005JD006655, 2006.

Gaudel, A., Ancellet, G., and Godin-Beekmann, S.: Analysis of 20 years of tropospheric ozone vertical profiles by lidar and ECC at Observatoire de Haute Provence (OHP) at 44° N, 6.7° E, Atmos. Environ., 113, 78–89, https://doi.org/10.1016/j.atmosenv.2015.04.028, 2015.

Godin, S., Carswell, A. I., Donovan, D. P., Claude, H., Steinbrecht, W., McDermid, I. S., McGee, T. J., Gross, M. R., Nakane, H., Swart, D. P. J., Bergwerff, H. B., Uchino, O., von der Gathen, P., and Neuber, R: Ozone differential absorption lidar algorithm intercomparison, Appl. Optics, 38, 6225–6236, 1999.

Harris N., Hudson, R. D., and Phillips, C. (Eds.): WMO, SPARC/IOC/GAW Ozone Profile Trend Assessment, WMO Global Ozone Research and Monitoring Project – Report No. 43, Geneva, 1998.

Hase, F., Blumenstock, T., and Paton-Walsh, C.: Analysis of the instrumental line shape of high-resolution Fourier transform IR spectrometers with gas cell measurements and new retrieval software, Appl. Optics, 38, 3417–3422, 1999.

Hinkley, E. D.: Laser monitoring of the atmosphere, Topics in applied physics, 14, Springer-Verlag, New York, 380 pp., 1976.

Hoareau, C., Keckhut, P., Baray, J.-L., Robert, L., Courcoux, Y., Porteneuve, J., Vömel, H., and Morel, B.: A Raman lidar at La Reunion (20.8° S, 55.5° E) for monitoring water vapour and cir-

rus distributions in the subtropical upper troposphere: preliminary analyses and description of a future system, Atmos. Meas. Tech., 5, 1333–1348, https://doi.org/10.5194/amt-5-1333-2012, 2012.

Hurtmans, D., Coheur, P.-F., Wespes, C., Clarisse, L., Scharf, O., Clerbaux, C., Hadji-Lazaro, J., George, M., and Turquety, S.: FORLI radiative transfer and retrieval code for IASI, J. Quant. Spectrosc. Ra., 113, 1391–1408, https://doi.org/10.1016/j.jqsrt.2012.02.036, 2012.

Johnson, B. J., Oltmans, S. J., Vömel, H., Smit, H. G. J., Deshler, T., and Kroeger, C.: ECC Ozonesonde pump efficiency measurements and tests on the sensitivity to ozone of buffered and unbuffered ECC sensor cathode solutions, J. Geophys. Res.-Atmos., 107, 4393, https://doi.org/10.1029/2001JD000557, 2002.

Johnson, B. J., Oltmans, S. J., Vömel, H., Smit, H. G. J., Deshler, T., and Kroeger, C.: Sensor solutions for the ECC ozonesondes, WMO-GAW-SHADOZ-NDACC Ozone Sonde Experts Workshop, Edinburgh, Scotland, 2016.

Keckhut, P., McDermid, S., Swart, D., McGee, T., Godin-Beekmann, S., Adriani, A., Barnes, J., Baray, J.-L., Bencherif, H., Claude, H., di Sarra, A. G., Fiocco, G., Hansen, G., Hauchecorne, A., Leblanc, T., Hie Lee, C., Pal, S., Megie, G., Nakane, H., Neuber, R., Steinbrechth, W., and Thayero, J.: Review of ozone and temperature lidar validations performed within the framework of the Network for the Detection of Stratospheric Change, J. Environ. Monitor., 6, 721–733, 2004.

Keckhut, P., Courcoux, Y., Baray, J.-L., Porteneuve, J., Vérèmes, H., Hauchecorne, A., Dionisi, D., Posny, F., Cammas, J.-P., Payen, G., Gabarrot, F., Evan, S., Khaykin, S., Rüfenacht, R., Tschanz, B., Kämpfer, N., Ricaud, P., Abchiche, A., Leclair-de-Bellevue, J., and Duflot, V.: Introduction to the Maïdo Lidar Calibration Campaign dedicated to the validation of upper air meteorological parameters, J. Appl. Remote Sens., 9, 094099, https://doi.org/10.1117/1.JRS.9.094099, 2015.

Khaykin S., Hauchecorne, A., Porteneuve, J., Mariscal, J.-F., D'Almeida, E., Cammas, J.-P., Payen, G., Evan, S., and Keckhut, P.: Ground-based Rayleigh-Mie Doppler lidar for wind measurements in the middle atmospheres, The 27th International Laser Radar Conference (ILRC 27), EPJ Web of Conferences, 119, 13005, https://doi.org/10.1051/epjconf/201611913005, 2016.

Komhyr, W. D., Barnes, R. A., Brothers, G. B., Lathrop, J. A., and Opperman, D. P: Electrochemical concentration cell ozonesonde performance evaluation during STOIC 1989, J. Geophys. Res.-Atmos., 100, 9231–9244, 1995.

Kovalev, V. A. and Eichinger, W. E.: Elastic Lidar: Theory, Practice, and Analysis Methods, Wiley Edition, ISBN: 978-0-471-20171-7, 2004.

Lacis, A. A., Wuebbles, D. J., and Logan, J. A.: Radiative Forcing of Climate by Changes in the Vertical Distribution of Ozone, J. Geophys. Res.-Atmos., 95, 9971–9981, https://doi.org/10.1029/JD095iD07p09971, 1990.

Leblanc, T., Sica, R. J., van Gijsel, J. A. E., Godin-Beekmann, S., Haefele, A., Trickl, T., Payen, G., and Gabarrot, F.: Proposed standardized definitions for vertical resolution and uncertainty in the NDACC lidar ozone and temperature algorithms – Part 1: Vertical resolution, Atmos. Meas. Tech., 9, 4029–4049, https://doi.org/10.5194/amt-9-4029-2016, 2016a.

Leblanc, T., Sica, R. J., van Gijsel, J. A. E., Godin-Beekmann, S., Haefele, A., Trickl, T., Payen, G., and Liberti, G.: Proposed standardized definitions for vertical resolution and uncertainty in the NDACC lidar ozone and temperature algorithms – Part 2: Ozone DIAL uncertainty budget, Atmos. Meas. Tech., 9, 4051–4078, https://doi.org/10.5194/amt-9-4051-2016, 2016b.

Leclair De Bellevue J., Réchou A., Baray J.-L., Ancellet G., and Diab, R. D.: Signatures of stratosphere to troposphere transport near deep convective events in the southern subtropics, J. Geophys. Res.-Atmos., 111, D24107, https://doi.org/10.1029/2005JD006947, 2006.

Martin, R. V., Jacob, D. J. , Yantosca, R. M., Chin, M., and Ginoux, P.: Global and regional decreases in tropospheric oxidants from photochemical effects of aerosols, J. Geophys. Res.-Atmos., 108, 4097, https://doi.org/10.1029/2002JD002622, 2003.

McGee, T. J., Gross, M., Ferrare, R., Heaps, W., and Singh, U.: Raman dial measurements of stratospheric ozone in the presence of volcanic aerosols, Geophys. Res. Lett., 20, 955–958, https://doi.org/10.1029/93GL00751, 1993.

Molina, L. T. and Molina, M. J.: Absolute absorption cross sections of ozone in the 185- to 350-nm wavelength range, J. Geophys. Res.-Atmos., 91, 14501–14508, https://doi.org/10.1029/JD091iD13p14501, 1986.

Morel, B., Bencherif, H., Keckhut, P., Baldy, S., and Hauchecorne, A.: Evidence of tidal perturbations in the middle atmosphere over Southern Tropics as deduced from LIDAR data analyses, J. Atmos. Sol.-Terr. Phy., 64, 1979–1988, https://doi.org/10.1016/S1364-6826(02)00223-7, 2002.

Network for the Detection of Atmospheric Composition Change: Network for the Detection of Atmospheric Composition Change (NDACC), NOAA / National Weather Service, National Centers for Environmental Prediction, Climate Prediction Center 5830, University Research Court College Park, MD 207402017, USA, available at: http://www.ndsc.ncep.noaa.gov/, last access: 5 September 2017.

Pelon J.: Distribution verticale de l'ozone dans la troposphère et la stratosphère: étude expérimentale par télédétection laser et application aux échanges troposphère-stratosphère, Thèse de l'Université Paris 06, 1985.

Portafaix, T., Morel, B., Bencherif, H., Baldy, S., Godin-Beekmann, S., and Hauchecorne, A.: Fine-scale study of a thick stratospheric ozone lamina at the edge of the southern subtropical barrier, J. Geophys. Res., 108, 4196, https://doi.org/10.1029/2002JD002741, 2003.

Portafaix T., Godin-Beekmann, S., Payen, G., de Mazière, M., Langerock, B., Fernandez, S., Posny, F., Cammas, J. P., Metzger, J. M., Bencherif, H., Vigouroux, C., and Marquestaut, N.: Ozone profiles obtained by DIAL technique at Maïdo Observatory in La Reunion Island: comparisons with ECC ozone-sondes, ground-based FTIR spectrometer and microwave radiometer measurements, ILRC 27, EPJ Web of Conferences, 119, 05005, https://doi.org/10.1051/epjconf/201611905005, 2016.

Posny, F., Johnson, B. J., Metzger, J.-M., Duflot, V., Portafaix, T., Cullis, P., Thompson, A. M., and Witte, J. C.: La Reunion Island (21° S, 55.5° E) SHADOZ/NDACC station: First re-processed ozonesonde data and comparisons with lidar measurements at the Maïdo Observatory, Quadriennial Ozone Symposium of the International Ozone Commission, QOS2016-192, Edinburgh, Scotland, 2016.

Rodgers, C. D.: Inverse Methods for Atmospheric Sounding: Theory and Practice, Series on Atmospheric, Oceanic and Planetary Physics, vol. 2, World Scientific, Singapore, 2000.

Rodgers, C. D. and Connor, B. J.: Intercomparison of remote sounding instruments, J. Geophys. Res.-Atmos., 108, 4116, https://doi.org/10.1029/2002JD002299, 2003.

Savitzky, A. and Golay, M. J. E.: Smoothing and Differentiation of Data by Simplified Least Squares Procedures, Anal. Chem., 36, 1627–1639, https://doi.org/10.1021/ac60214a047, 1964.

Sivakumar, V., Vishnu Prasanth, P., Kishore, P., Bencherif, H., and Keckhut, P.: Rayleigh LIDAR and satellite (HALOE, SABER, CHAMP and COSMIC) measurements of stratosphere-mesosphere temperature over a southern sub-tropical site, Reunion (20.8° S; 55.5° E): climatology and comparison study, Ann. Geophys., 29, 649–662, https://doi.org/10.5194/angeo-29-649-2011, 2011a.

Sivakumar, V., Bencherif, H., Bègue, N., and Thompson, A. N.: Tropopause Characteristics and Variability from 11 yr of SHADOZ Observations in the Southern Tropics and Subtropics, J. Appl. Meteorol. Clim., 50, 1403–1416, https://doi.org/10.1175/2011JAMC2453.1, 2011b.

Smit, H. G. J., Straeter, W., Johnson, B. J., Oltmans, S. J., Davies, J., Tarasick, D. W., Hoegger, B., Stubi, R., Schmidlin, F. J., Northam, T., Thompson, A. M., Witte, J. C., Boyd, I., and Posny, F.: Assessment of the performance of ECC-ozonesondes under quasi-flight conditions in the environmental simulation chamber: Insights from the Juelich Ozone Sonde Intercomparison Experiment (JOSIE), J. Geophys. Res., 112, D19306, https://doi.org/10.1029/2006JD007308, 2007.

Smit, H. G. J., Oltmans, S., Deshler, T., Tarasick, D., Johnson, B., Schmidlin, F., Stuebi, R., and Davies, J.: O3S-DQA Activity: Guide Lines for homogenization of ozone sonde data, Activity as part of SPARC-IGACO-IOC Assessment (SI2N) "Past Changes in the Vertical Distribution of Ozone", available at: http://www-das.uwyo.edu/~deshler/NDACC_O3Sondes/O3s_DQA/O3S-DQA-GuidelinesHomogenization-V2-19November2012.pdf (last access: 28 August 2017), 2012.

Stevenson, D. S., Dentener, F. J., Schultz, M. G., Ellingsen, K., van Noije, T. P. C., Wild, O., Zeng, G., Amann, M., Atherton, C. S., Bell, N., Bergmann, D. J., Bey, I., Butler, T., Cofala, J., Collins, W. J., Derwent, R. G., Doherty, R. M., Drevet, J., Eskes, H. J., Fiore, A. M., Gauss, M., Hauglustaine, D. A., Horowitz, L. W., Isaksen, I. S. A., Krol, M. C., Lamarque, J.-F., Lawrence, M. G., Montanaro, V., Müller, J.-F., Pitari, G., Prather, M. J., Pyle, J. A., Rast, S., Rodriguez, J. M., Sanderson, M. G., Savage, N. H., Shindell, D. T., Strahan, S. E., Sudo, K., and Szopa, S.: Multimodel ensemble simulations of presentday and near-future tropospheric ozone, J. Geophys. Res.-Atmos., 111, D08301, https://doi.org/10.1029/2005JD006338, 2006.

Sullivan, J. T., McGee, T. J., DeYoung, R., Twigg, L. W., Sumnicht, G. K., Pliutau, D., Knepp, T., and Carrion, W.: Results from the NASA GSFC and LaRC Ozone Lidar Intercomparison: New Mobile Tools for Atmospheric Research, J. Atmos. Ocean. Tech., 32, 1779–1795, https://doi.org/10.1175/JTECH-D-14-00193.1, 2015.

Thompson, A. M., Balashov, N. V., Witte, J. C., Coetzee, J. G. R., Thouret, V., and Posny, F.: Tropospheric ozone increases over the southern Africa region: bellwether for rapid growth in Southern Hemisphere pollution?, Atmos. Chem. Phys., 14, 9855–9869, https://doi.org/10.5194/acp-14-9855-2014, 2014.

Uchino, O., Sakai, T., Nagai, T., Morino, I., Maki, T., Deushi, M., Shibata, K., Kajino, M., Kawasaki, T., Akaho, T., Takubo, S., Okumura, H., Arai, K., Nakazato, M., Matsunaga, T., Yokota, T., Kawakami, S., Kita, K., and Sasano, Y.: DIAL measurement of lower tropospheric ozone over Saga (33.24° N, 130.29° E), Japan, and comparison with a chemistry–climate model, Atmos. Meas. Tech., 7, 1385–1394, https://doi.org/10.5194/amt-7-1385-2014, 2014.

Vérèmes, H., Cammas, J.-P., Baray, J.-L., Keckhut, P., Barthe, C., Posny, F., Tulet, P., Dionisi, D., and Bielli, S.: Multiple subtropical stratospheric intrusions over Reunion Island: Observational, Lagrangian, and Eulerian numerical modeling approaches, J. Geophys. Res., 121, 14414–14432, https://doi.org/10.1002/2016JD025330, 2016.

Vérèmes, H., Payen, G., Keckhut, P., Duflot, V., Baray, J.-L., Cammas, J.-P., Leclair De Bellevue, J., Evan, S., Posny, F., Gabarrot, F., Metzger, J.-M., Marquestaut, N., Meier, S., Vömel, H., and Dirksen, R.: A Raman lidar at Maïdo Observatory (Reunion Island) to measure water vapor in the troposphere and lower stratosphere: calibration and validation, Atmos. Meas. Tech. Discuss., https://doi.org/10.5194/amt-2017-32, in review, 2017.

Vigouroux, C., De Mazière, M., Demoulin, P., Servais, C., Hase, F., Blumenstock, T., Kramer, I., Schneider, M., Mellqvist, J., Strandberg, A., Velazco, V., Notholt, J., Sussmann, R., Stremme, W., Rockmann, A., Gardiner, T., Coleman, M., and Woods, P.: Evaluation of tropospheric and stratospheric ozone trends over Western Europe from ground-based FTIR network observations, Atmos. Chem. Phys., 8, 6865–6886, https://doi.org/10.5194/acp-8-6865-2008, 2008.

Vigouroux, C., Blumenstock, T., Coffey, M., Errera, Q., García, O., Jones, N. B., Hannigan, J. W., Hase, F., Liley, B., Mahieu, E., Mellqvist, J., Notholt, J., Palm, M., Persson, G., Schneider, M., Servais, C., Smale, D., Thölix, L., and De Mazière, M.: Trends of ozone total columns and vertical distribution from FTIR observations at eight NDACC stations around the globe, Atmos. Chem. Phys., 15, 2915–2933, https://doi.org/10.5194/acp-15-2915-2015, 2015.

Witte, J. C., Thompson, A. M., Smit, H. G. J., Fujiwara, M., Posny, F., Coetzee, G. J. R., Northam, E. T., Johnson, B. J., Sterling, C. W., Mohammed, M., Ogino, S.-Y., Jordan, A., Zainel, Z., and da Silva, F. R.: First reprocessing of Southern Hemisphere ADditional OZonesondes (SHADOZ) profile records (1998–2015): 1. Methodology and evaluation, J. Geophys. Res.-Atmos., 122, 6611–6636, https://doi.org/10.1002/2016JD026403, 2017.

Zhou, M., Vigouroux, C., Langerock, B., Wang, P., Dutton, G., Hermans, C., Kumps, N., Metzger, J.-M., Toon, G., and De Mazière, M.: CFC-11, CFC-12 and HCFC-22 ground-based remote sensing FTIR measurements at Réunion Island and comparisons with MIPAS/ENVISAT data, Atmos. Meas. Tech., 9, 5621–5636, https://doi.org/10.5194/amt-9-5621-2016, 2016.